

# Quantum correlation in the photoassociation of a heteronuclear molecular Bose-Einstein Condensate

Lu Zhou<sup>1,2,3,4</sup>, Weiping Zhang<sup>1\*</sup>

<sup>1</sup>*Key Laboratory of Optical and Magnetic Resonance Spectroscopy (Ministry of Education), Department of Physics, East China Normal University, Shanghai 200062, P. R. China*

<sup>2</sup>*State Key Laboratory of Magnetic Resonance and Atomic and Molecular Physics, Wuhan Institute of Physics and Mathematics, Chinese Academy of Sciences, Wuhan 430071, P. R. China*

<sup>3</sup>*Center for Cold Atom Physics, Chinese Academy of Sciences, Wuhan 430071, P. R. China and*

<sup>4</sup>*Graduate School of the Chinese Academy of Sciences, Wuhan 430071, P. R. China*

Hong Y. Ling<sup>1,5</sup>

<sup>5</sup>*Department of Physics and Astronomy, Rowan University, Glassboro, New-Jersey, 08028-1700, USA*

Han Pu

*Department of Physics and Astronomy, and Rice Quantum Institute, Rice University, Houston, TX 77251-1892, USA*

We study a atomic-molecular model for interspecies photoassociation. A general Hamiltonian which takes into account the s-wave scattering interactions are considered. By approximating the quantum Hamiltonian by a classical Hamiltonian, the fixed points of the system are found. The stability analysis is performed and we found that the population imbalance between the two atomic species will play an important role in the modulational instability of the system. It is found that efficient photoassociation could be achieved in wider experimental parameter region with population imbalance. The dynamics of the system is predicted with mean-field theory as well as with quantum solution. The difference between them are found and analyzed. In addition, we give a brief discussion on the role of the quantum statistical properties of the initial atomic condensate state on the dynamics of the system. The time evolution of the correlation between atoms of different species are calculated with different initial states and we found that the two species can be kept anti-correlated under appropriate conditions. We also numerically show that quantum statistical properties of the matter wave field changes due to the nonlinear interaction.

PACS numbers: 03.75.-b, 05.30.Jp

## I. INTRODUCTION

The creation of ultracold molecules from ultracold atoms by the means of magnetic Feshbach resonances or photoassociation has been the focus of experimental [1–6] and theoretical research [7–18] during the last years. Both ultracold degenerate Bose and Fermi atoms have been successfully converted into molecules. A lot of theoretical work have been devoted to improving the conversion efficiency [7–10], studying the dynamics of the atom-molecular coupling model [11–18] and molecular dissociation [19].

On the other hand, atomic mixtures of different species such as two-component Bose-Einstein condensate or Bose-Fermi mixtures are under intense attention for their rich dynamics and the potential application in experiments. It has drawn much theoretical interest such as the dynamics and Berry phase of the two-species Bose-Einstein condensates [20–23], as well as the phonon spectrum and dynamical stability of Bose-Fermi mixture [24].

Specifically, recent experiments on heteronuclear Feshbach resonance [1–3] or photoassociation [4–6] have opened up the gate to create ultracold heteronuclear molecules with atoms of different species. Ultracold heteronuclear molecules composed of two-species alkali atoms such as KRb, RbCs and NaCs are successfully created in experiments. The ultracold heteronuclear molecules have attracted much interest for their potential applications in the investigation of quantum computation and fundamental symmetries.

The dynamics of heteronuclear photoassociation of Bose atoms of different species, have not been investigated in detail according to our knowledge. The only work covering the subject [10], as we know, is focus on the Feshbach-assisted photoassociation and does not take into account the s-wave scattering interactions and population imbalance between the atomic condensates.

In the present work we will study a simple atomic-molecular model for interspecies photoassociation. A general Hamiltonian which takes into account the s-wave scattering interactions are considered. By approximating the quantum Hamiltonian by a classical Hamiltonian, the fixed points of the system are found. The stability analysis is performed and we found that the population imbalance will play an important role in the modulational in-

---

\*To whom correspondence should be addressed E-mail: wpzhang@phy.ecnu.edu.cn

stability of the system. It is found that efficient photoassociation could be achieved in wider experimental parameter region with population imbalance. The dynamics of the system is predicted with mean-field theory as well as with quantum solution. The difference between them are found and analyzed. We also give a brief discussion on the role of the quantum statistical properties of the initial atomic condensate state on the dynamics of the system. The time evolution of the correlation between atoms of different species are calculated with different initial states and we found that the two species can be kept anti-correlated under appropriate conditions. We also numerically show that quantum statistical properties of the matter wave field changes due to the nonlinear interaction.

The paper is organized as follows. In Sec. 2 we present the model and study the dynamics with mean-field theory as well as with quantum solution. By making the classical analogue of the model, we determined the fixed points of the system and their modulational instability is analyzed. In Sec. 3 we discuss the quantum correlation and statistical properties of the matter wave field during the dynamical evolution and conclude in Sec. 4.

## II. MODEL AND DYNAMICS

We consider the zero-temperature Bose-Einstein condensate system in which the bosonic atoms of species 1 and 2 are coupled to molecular condensate  $b$  via interspecies photoassociation. The condensate of different species interact with themselves and each other via s-wave elastic collisions. In the formalism of the vector quantum field theory [28], the Hamiltonian of the system can be written as

$$\hat{H} = \hat{H}_0 + \hat{H}_{int} + \hat{H}_{couple} \quad (1)$$

$$\begin{aligned} \hat{H}_0 = & \sum_{i=1,2} \int d\mathbf{r} \hat{\psi}_i^\dagger(\mathbf{r}) \left[ -\frac{\hbar^2}{2m_i} \nabla^2 + V_i(\mathbf{r}) \right. \\ & \left. + U_i \hat{\psi}_i^\dagger(\mathbf{r}) \hat{\psi}_i(\mathbf{r}) \right] \hat{\psi}_i(\mathbf{r}) \\ & + \int d\mathbf{r} \hat{\psi}_b^\dagger(\mathbf{r}) \left[ -\frac{\hbar^2}{2m_b} \nabla^2 + V_b(\mathbf{r}) \right. \\ & \left. + \Delta_b + U_b \hat{\psi}_b^\dagger(\mathbf{r}) \hat{\psi}_b(\mathbf{r}) \right] \hat{\psi}_b(\mathbf{r}) \end{aligned} \quad (2)$$

$$\hat{H}_{int} = \sum_{\substack{i,j=1,2,b \\ i \neq j}} U_{ij} \int d\mathbf{r} \hat{\psi}_i^\dagger(\mathbf{r}) \hat{\psi}_j^\dagger(\mathbf{r}) \hat{\psi}_j(\mathbf{r}) \hat{\psi}_i(\mathbf{r}) \quad (3)$$

$$\hat{H}_{couple} = \lambda \int d\mathbf{r} \left[ \hat{\psi}_b^\dagger(\mathbf{r}) \hat{\psi}_1(\mathbf{r}) \hat{\psi}_2(\mathbf{r}) + H.c. \right] \quad (4)$$

where  $\hat{\psi}_i(\mathbf{r})$  are quantum field operators of different species which obey the following equal-time commuta-

tion relations

$$\begin{aligned} [\hat{\psi}_i(\mathbf{r}), \hat{\psi}_j(\mathbf{r}')] &= [\hat{\psi}_i^\dagger(\mathbf{r}), \hat{\psi}_j^\dagger(\mathbf{r}')] = 0 \\ [\hat{\psi}_i(\mathbf{r}), \hat{\psi}_j^\dagger(\mathbf{r}')] &= \delta_{ij} \delta(\mathbf{r} - \mathbf{r}') \end{aligned} \quad (5)$$

One can see that  $\hat{H}_0$  describe the dynamics of each condensate without interspecies interaction,  $V_i(\mathbf{r})$  is the trapping potential and  $U_i = 4\pi\hbar^2 a_i/m_i$ , where  $a_i$  is the s-wave scattering length of condensate  $i$  and  $\Delta_b > 0$  corresponds to tuning of the laser by the energy  $\Delta_b$  above the photoassociation threshold.  $\hat{H}_{int}$  stand for the interaction between different species via s-wave elastic scattering with  $U_{ij} = 2\pi\hbar^2 a_{ij}/M_{ij}$ , where  $a_{ij}$  is the s-wave scattering length between different species and the reduced mass  $M_{ij} = m_i m_j / (m_i + m_j)$ . The interspecies photoassociation process is incorporated in  $\hat{H}_{couple}$  with the coupling constant  $\lambda$ .

It is familiar that at zero temperature the field operators can be approximated as [20, 21, 29]

$$\hat{\psi}_{1(2)}(\mathbf{r}) \approx \hat{a}_{1(2)} \Phi_{1(2)}(\mathbf{r}), \hat{\psi}_b(\mathbf{r}) \approx \hat{b} \Phi_b(\mathbf{r}) \quad (6)$$

Insert Eq. (6) into Eq. (1) we can have

$$\begin{aligned} \hat{H} = & \delta \hat{b}^\dagger \hat{b} + g \left( \hat{b}^\dagger \hat{a}_1 \hat{a}_2 + H.c. \right) \\ & + \chi_1 \hat{a}_1^\dagger \hat{a}_1^\dagger \hat{a}_1 \hat{a}_1 + \chi_2 \hat{a}_2^\dagger \hat{a}_2^\dagger \hat{a}_2 \hat{a}_2 + \chi_b \hat{b}^\dagger \hat{b}^\dagger \hat{b} \hat{b} \\ & + \chi_{12} \hat{a}_1^\dagger \hat{a}_1 \hat{a}_2^\dagger \hat{a}_2 + \chi_{b1} \hat{a}_1^\dagger \hat{a}_1 \hat{b}^\dagger \hat{b} + \chi_{b2} \hat{a}_2^\dagger \hat{a}_2 \hat{b}^\dagger \hat{b} \end{aligned} \quad (7)$$

with

$$\begin{aligned} \delta = & \int d\mathbf{r} \left[ -\frac{\hbar^2}{2m_b} |\nabla \Phi_b(\mathbf{r})|^2 + V_b(\mathbf{r}) |\Phi_b(\mathbf{r})|^2 \right] + \Delta_b \\ - \sum_{i=1,2} \int d\mathbf{r} \left[ -\frac{\hbar^2}{2m_i} |\nabla \Phi_i(\mathbf{r})|^2 + V_i(\mathbf{r}) |\Phi_i(\mathbf{r})|^2 \right] \end{aligned} \quad (8)$$

$$g = \lambda \int d\mathbf{r} \Phi_b^*(\mathbf{r}) \Phi_1(\mathbf{r}) \Phi_2(\mathbf{r}) \quad (9)$$

and

$$\chi_i = U_i \int d\mathbf{r} |\Phi_i(\mathbf{r})|^4, \chi_{ij} = U_{ij} \int d\mathbf{r} |\Phi_i(\mathbf{r})|^2 |\Phi_j(\mathbf{r})|^2 \quad (10)$$

One can see from Eq. (7) that without the nonlinear terms our model will reduce to the trilinear Hamiltonian which was used to investigate nondegenerate parametric down-conversion in quantum optics [25, 26]. We note two quantities are conserved by the Hamiltonian (7):

$$N = \hat{a}_1^\dagger \hat{a}_1 + \hat{a}_2^\dagger \hat{a}_2 + 2\hat{b}^\dagger \hat{b}, D = \hat{a}_1^\dagger \hat{a}_1 - \hat{a}_2^\dagger \hat{a}_2 \quad (11)$$

which accounts for the total particle number and the number difference between the two atomic species, respectively. To investigate the dynamics, similar to [14], we

introduce the following pseudoangular momentum operators

$$\hat{L}_x = \sqrt{2} \frac{\hat{b}^\dagger \hat{a}_1 \hat{a}_2 + \hat{a}_1^\dagger \hat{a}_2^\dagger \hat{b}}{N^{3/2}} \quad (12)$$

$$\hat{L}_y = \sqrt{2} \frac{\hat{a}_1^\dagger \hat{a}_2^\dagger \hat{b} - \hat{b}^\dagger \hat{a}_1 \hat{a}_2}{i N^{3/2}} \quad (13)$$

$$\hat{L}_z = \frac{\hat{a}_1^\dagger \hat{a}_1 + \hat{a}_2^\dagger \hat{a}_2}{N} \quad (14)$$

It is clear that  $\langle \hat{L}_z \rangle$  has the physical meaning of normalized atomic number. It should be note that the three operators do not represent  $SU(2)$ , they obey the following commutation relations

$$[\hat{L}_x, \hat{L}_y] = \frac{1}{iN} (d^2 + 2\hat{L}_z - 3\hat{L}_z^2) + \frac{2}{iN^2} (1 - \hat{L}_z) \quad (15)$$

$$[\hat{L}_y, \hat{L}_z] = \frac{2i}{N} \hat{L}_x, [\hat{L}_z, \hat{L}_x] = \frac{2i}{N} \hat{L}_y \quad (16)$$

where  $d = D/N$  is also a constant of motion.

With the three operators Hamiltonian (7) can be rewritten as (discarding the constant terms)

$$\hat{H} = G \left( \frac{N}{2} \hat{L}_x + \frac{N\Lambda}{4} \hat{L}_z^2 - \frac{N\Delta}{2} \hat{L}_z \right) \quad (17)$$

where

$$\begin{aligned} \Lambda &= (\Lambda_1 + \Lambda_2 + \Lambda_b + \Lambda_{12} - \Lambda_{b1} - \Lambda_{b2})/G \\ \Delta &= [\delta - (d - 1/N) \Lambda_1 + (d + 1/N) \Lambda_2 \\ &\quad + (1 - 1/N) \Lambda_b - (1 - d) \Lambda_{b1}/2 - (1 + d) \Lambda_{b2}/2] \end{aligned} \quad (18)$$

with  $G = g\sqrt{2N}$  and  $\Lambda_i = N\chi_i$ . The Heisenberg equation of the three operators can be derived as (with the normalized time  $\tau = Gt$ )

$$\begin{aligned} \frac{d}{d\tau} \hat{L}_x &= -\frac{\Lambda}{2} (\hat{L}_y \hat{L}_z + \hat{L}_z \hat{L}_y) + \Delta \hat{L}_y \\ \frac{d}{d\tau} \hat{L}_y &= \frac{\Lambda}{2} (\hat{L}_x \hat{L}_z + \hat{L}_z \hat{L}_x) - \Delta \hat{L}_x \\ &\quad + (d^2 + 2\hat{L}_z - 3\hat{L}_z^2)/2 + (1 - \hat{L}_z)/N \\ \frac{d}{d\tau} \hat{L}_z &= \hat{L}_y \end{aligned} \quad (19)$$

Use the mean-field approximation then we can take  $\langle \hat{L}_i \hat{L}_j \rangle = \langle \hat{L}_i \rangle \langle \hat{L}_j \rangle$ , from Eqs. (15) and (16), we can see this approximation is correct once the partical number  $N$  is large enough for the safe ignoring of the terms

propotional to  $1/N$ . Then we have

$$\begin{aligned} \frac{d}{d\tau} \langle \hat{L}_x \rangle &= -\Lambda \langle \hat{L}_y \rangle \langle \hat{L}_z \rangle + \Delta \langle \hat{L}_y \rangle \\ \frac{d}{d\tau} \langle \hat{L}_y \rangle &= \Lambda \langle \hat{L}_x \rangle \langle \hat{L}_z \rangle - \Delta \langle \hat{L}_x \rangle \\ &\quad + (d^2 + 2\langle \hat{L}_z \rangle - 3\langle \hat{L}_z \rangle^2)/2 \\ \frac{d}{d\tau} \langle \hat{L}_z \rangle &= \langle \hat{L}_y \rangle \end{aligned} \quad (20)$$

note that we have neglected the  $O(1/N)$  terms in Eq.(20), such terms are also be neglected in  $\Delta$ .

Eq. (20) can be easily solved with Runge-Kutta algorithm under the initial condition  $(\langle \hat{L}_x \rangle, \langle \hat{L}_y \rangle, \langle \hat{L}_z \rangle) = (0, 0, 1)$ . However, to gain insight of the dynamics, we first resort to the classical analysis, which was frequently used to discuss the model for the coupling of molecular condensate with single species atomic condensate [15–17]. It is done by replacing the quantum operators  $\hat{i}$  ( $i = a_1, a_2, b$ ) by the complex numbers  $\sqrt{\langle N_i \rangle} e^{i\varphi_i}$ . By introducing two conjugate variables  $x = (N_1 + N_2)/N$  and  $\varphi = \varphi_1 + \varphi_2 - \varphi_b$ , from Eq. (7) we can derive the canonical Hamiltonian with the scaled time  $\tau = Gt$  (in the limit of large particle number  $N$ )

$$H = \Delta x - \frac{\Lambda}{2} x^2 - \sqrt{(1-x)(x^2-d^2)} \cos \varphi \quad (21)$$

We note that if  $d = 0$ , Eq. (21) would have almost the same form as the corresponding equations in [16, 17]. With nonzero  $d$ , which has the physical meaning of population imbalance between the two atomic species, our model would display different dynamical properties.

The coupled canonical Hamiltonian equations for the conjugate variables  $x$  and  $\varphi$  can be derived from Eq. (21) as

$$\begin{aligned} \frac{dx}{d\tau} &= -\frac{\partial H}{\partial \varphi} = -\sqrt{(1-x)(x^2-d^2)} \sin \varphi \\ \frac{d\varphi}{d\tau} &= \frac{\partial H}{\partial x} = \Delta - \Lambda x - \frac{d^2 + 2x - 3x^2}{2\sqrt{(1-x)(x^2-d^2)}} \cos \varphi \end{aligned} \quad (22)$$

The fixed points  $(x_0, \varphi_0)$  correspond to steady-state solution can be found via the solution of  $dx/d\tau, d\varphi/d\tau|_{x_0, \varphi_0} = 0$ . In order to keep the particle number in each mode is greater than or equal to zero,  $x$  should be in the region  $[|d|, 1]$ , and  $d$  is in the region  $[-1, 1]$ . It can be seen from Eq. (22) that with  $d = 0$ , there exists pure molecular phase with  $x_0 = 0$ . While with nonzero  $d$  this fixed point no longer exists, the physical meaning is very clear that atoms can not be converted to molecular completely with population imbalance. Besides this, there are two types of fixed points, which is in-phase type of steady state with  $\varphi_0 = 0$  and out-of-phase type of steady state with  $\varphi_0 = \pi$ . The value of  $x_0$  can be determined by numerical solution of Eq. (22) with the corresponding  $\varphi_0$ .

Then there comes the natural question whether the steady states are stable, the stability analysis is performed by substituting  $x = x_0 + \delta x$  and  $\varphi = \varphi_0 + \delta\varphi$  into Eq.(22) and omitting the terms of the order greater than  $O(\delta x, \delta\varphi)$ , then we have

$$\begin{aligned} \frac{d}{d\tau} \delta x &= -\sqrt{(1-x_0)(x_0^2-d^2)} \cos \varphi_0 \delta\varphi \\ \frac{d}{d\tau} \delta\varphi &= \left\{ -\Lambda - \frac{(1-3x_0)}{\sqrt{(1-x_0)(x_0^2-d^2)}} \cos \varphi_0 \right. \\ &\quad \left. + \frac{(d^2+2x_0-3x_0^2)^2}{4[(1-x_0)(x_0^2-d^2)]^{3/2}} \cos \varphi_0 \right\} \delta x \end{aligned} \quad (23)$$

The oscillation frequency of  $\delta x$  and  $\delta\varphi$  can be derived straightforwardly as

$$\begin{aligned} \omega^2 &= \left[ \frac{(d^2+2x_0-3x_0^2)^2}{4(1-x_0)(x_0^2-d^2)} + 3x_0 - 1 \right] \cos^2 \varphi_0 \\ &\quad - \Lambda \sqrt{(1-x_0)(x_0^2-d^2)} \cos \varphi_0 \end{aligned} \quad (24)$$

The modulational instability occurs when  $\omega$  becomes imaginary ( $\omega^2 < 0$ ). The typical results from the stability analysis based on the parameters of our interest are summarized in Fig. 1, where the  $(\Lambda, \Delta)$  space is divided into the stable (white) and the unstable (dark) regions. The figures are for the in-phase fixed points, which are symmetric to the out-of-phase fixed points with the zero point  $\Lambda = \Delta = 0$ . Fig. 1(a) is for  $d = 0$ , one can see that the instability occurs for  $\Lambda > 1$  and  $\Delta > 1$ . Fig. 1(b) is for  $d = 0.2$  and Fig. 1(c) is for  $d = 0.5$ . We can see that the instability is caused by collision  $\Lambda$  and detuning  $\Delta$ , the modulational instability of the fixed points would not occur in the absence of them ( $\Lambda = \Delta = 0$ ). With the increase of the population imbalance, instability occurs for larger values of  $\Lambda$  and  $\Delta$ . To gain insight of the instability of the fixed points, it is useful to plot the level curves of the Hamiltonian (21). We choose the sample point of  $d = 0$ ,  $\Lambda = 2$  and  $\Delta = 1.2$  in Fig. 2(a). According to our calculations, there are two in-phase fixed points in this case, one is stable and the other one is unstable. It can be seen from the figure that the unstable one is the saddle point and the stable one is the minima. The situation becomes more complicated for  $d \neq 0$ , for the sample point of  $d = 0.2$ ,  $\Lambda = 3$  and  $\Delta = 2$  in Fig. 2(b), we found three in-phase fixed points, two local minima and one saddle point. The lower minima and the saddle point are unstable while the upper minima is stable. In Fig. 11 we show the value of both the in-phase and out-of-phase fixed points with respect to  $\Delta$ . Fig. 3(a) is for  $d = \Lambda = 0$ , it can be seen from the figure that in order to transfer atom to molecular efficiently for the steady state with  $\varphi_0 = 0$ , one could adiabatically tune  $\Delta$  from a high negative value to a positive value. For the steady state of  $\varphi_0 = \pi$   $\Delta$  should vary in an opposite direction. It should be noted that steady state solution with  $\varphi_0 = 0$  does not exist for  $\Delta > 1$ , and for  $\varphi_0 = \pi$  it does not exist

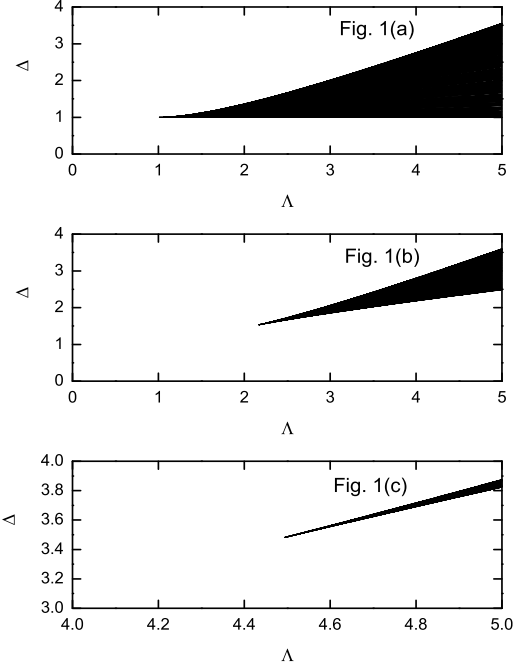


FIG. 1: Stability diagram for the in-phase fixed points in  $(\Lambda, \Delta)$  space. (a)  $d = 0$ ; (b)  $d = 0.2$ ; (c)  $d = 0.5$ .

for  $\Delta < -1$ . This means that inappropriate tuning of  $\Delta$  may cause detrimental effect to the conversion efficiency. Similar results were also discussed in [15]. Fig. 3(b) is for  $d = 0.2$  and  $\Lambda = 1$ , one can see that although not all atoms can be adiabatically transferred to molecular due to population imbalance, steady state solution exist in a much wider range of  $\Delta$  for both the in-phase and out-of-phase fixed points. This means we could achieve efficient heteronuclear photoassociation in wider experimental parameter region with population imbalance. All of the results above are in the stable region. In the following we would like to focus on the dynamics in the stable region ( $\Lambda > 0, \Delta = 0$ ). In Fig. 4 the value of  $x_0$  of the in-phase steady state is plotted with respect to  $\Lambda$  and  $d$ . The results are obtained by numerical solution of the nonlinear equation (22). The configuration of the out-of-phase fixed points is symmetric with Fig. 4 with respect to  $\Lambda = 0$  so we do not plot it here. Two results can be drawn from the figure: (1) the larger  $d$  is, the larger  $x_0$ . This is quite clear that more atoms will be remained with larger population imbalance. (2) the larger  $\Lambda$  is, the larger  $x_0$ . From Eq. (18) we can see that  $\Lambda$  estimates the strength of nonlinear collision, so this nonlinearity induced localization of atom population is analogous to the self-trapping in two component BEC [27]. Since our dynamics starts from  $x = 1$ , it can be predicted that the dynamical evolution will become more localized with increasing  $\Lambda$  and  $d$ . In Fig. 5(a) we solve Eq. (20) with  $\Delta = d = 0$ ,  $N = 2000$  and different values

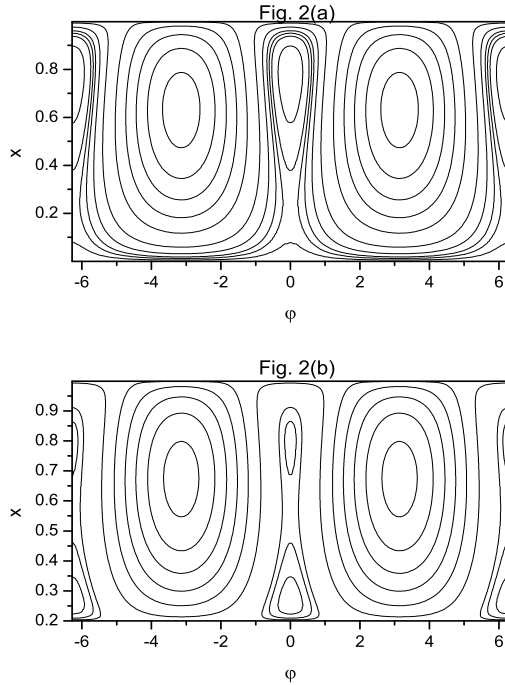


FIG. 2: Level curves of the Hamiltonian (a)  $d = 0$ ,  $\Lambda = 2$  and  $\Delta = 1.2$ ; (b)  $d = 0.2$ ,  $\Lambda = 3$  and  $\Delta = 2$ .

of  $\Lambda$ . Since the nonlinear collision parameters are kept unknown to us, throughout this paper we would choose  $\chi_1 = \chi_2 = \chi_{12} = \chi$ ,  $\chi_b = 2\chi$  and  $\chi_{b1} = \chi_{b2} = -1.5\chi$ . The time evolution of the normalized molecular population is plotted with  $\chi/g = 0$  ( $\Lambda = 0$ ),  $\chi/g = 10^{-3}$  ( $\Lambda = 0.1789$ ),  $\chi/g = 3 \times 10^{-3}$  ( $\Lambda = 0.5367$ ) as well as  $\chi/g = 6 \times 10^{-3}$  ( $\Lambda = 1.0733$ ). One can see that with  $\Lambda = 0$ , our system would evolve into the pure molecular phase. With the increase of the nonlinear interaction strength, molecular population will exhibit periodic oscillation, the oscillation frequency become higher and the amplitude become smaller. This means that the nonlinearity induce periodic conversion between atoms and molecular, it will also lead to self-trapping in the atomic condensate. In Fig. 5(b) we found quantum solution by diagonalize the Hamiltonian (7) and start from the initial state  $|(N+D)/2\rangle_1 |(N-D)/2\rangle_2 |0\rangle_b$ , the parameters are the same as that in Fig. 5(a). We found that in short time range the classical solution and the quantum solution are in good agreement. The quantum solution deviate from the classical solution in the sense that they exhibit damped oscillation, which is in analogy with a two-mode system coupled to an external reservoir. In Fig. 6 (a) and (b) we show classical and quantum solution for  $\Lambda = 0.1789$ ,  $N = 2000$  and different values of  $d$ . One can see that increasing  $d$  and increasing  $\Lambda$  have almost the same effect on the dynamics of the system, just as we have predicted in the previous discussion. Note that all the above parameters are chosen in

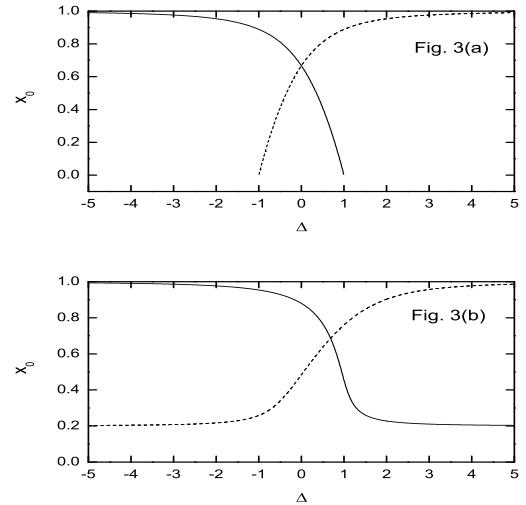


FIG. 3: Diagram of the value of  $x_0$  at the fixed points versus  $\Delta$ . The solid and dashed line corresponds to the in-phase ( $\varphi = 0$ ) and out-of-phase ( $\varphi = \pi$ ), respectively. (a)  $d = 0$ ,  $\Lambda = 0$ ; (b)  $d = 0.2$ ,  $\Lambda = 1$ .

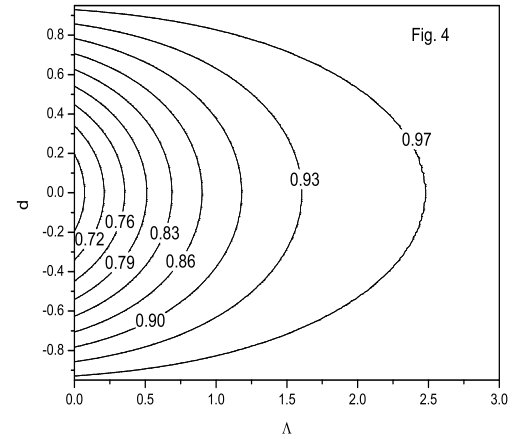


FIG. 4: Contour plot of the in-phase fixed points  $x_0$  with respect to  $\Lambda$  and  $d$ .

the steady region. Since it has been argued that in the process of Raman photoassociation of Bose Einstein condensates the quantum statistical properties of the initial state will play an important role [18], we would also like to give a brief discussion here. We calculate the quantum solution with the initial coherent state  $|\alpha\rangle_1 |\beta\rangle_2 |0\rangle_b$  as well as the Fock state, make their mean particle number equal to each other. In Fig. 7(a) the results for Fock state is presented, with 10 atoms in both species of the atomic condensate and  $\chi/g = 0.1$ . It can be seen from the figure that the molecular population exhibits oscillations.

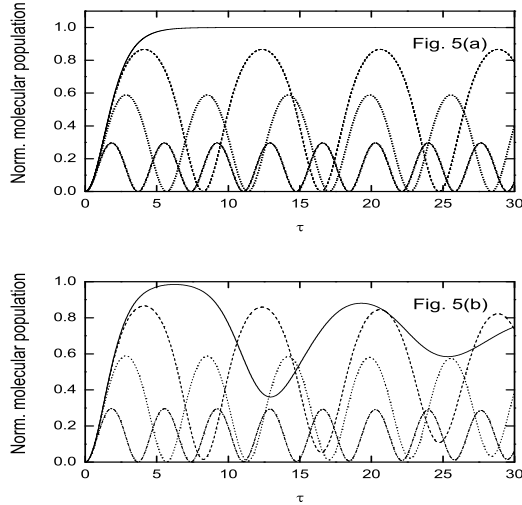


FIG. 5: Time evolution of the normalized molecular population for  $N = 2000$  and  $d = 0$ .  $\Lambda = 0$  (solid line),  $0.1789$  (dash line),  $0.5367$  (dot line) and  $1.0733$  (dash dot line) (a) mean-field solution. (b) quantum solution.

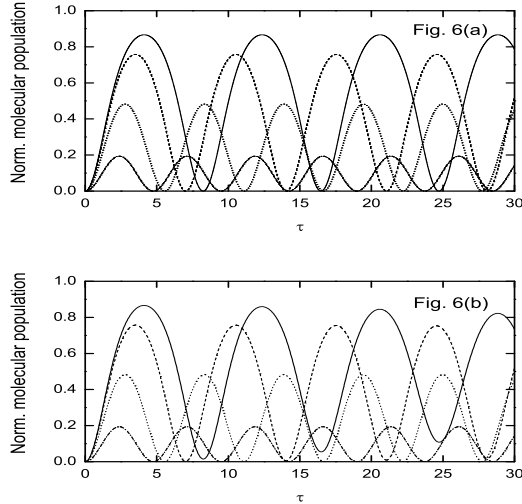


FIG. 6: Time evolution of the normalized molecular population for  $N = 2000$  and  $\Lambda = 0.1789$ .  $d = 0$  (solid line),  $0.2$  (dash line),  $0.5$  (dot line) and  $0.8$  (dash dot line) (a) mean-field solution. (b) quantum solution.

tion with periodically varying amplitude. This deviates from the mean-field prediction for our particle number is small and mean-field theory is valid in the large particle number limit. In Fig. 7(b) we present the result with the coherent state and  $\alpha = \beta = \sqrt{10}$ , it display quantitatively different behavior with the Fock state by periodically collapse and revival, which means the quantum statistical properties of the initial state really affect the dynamics of the system. In Fig. 8 we give the result

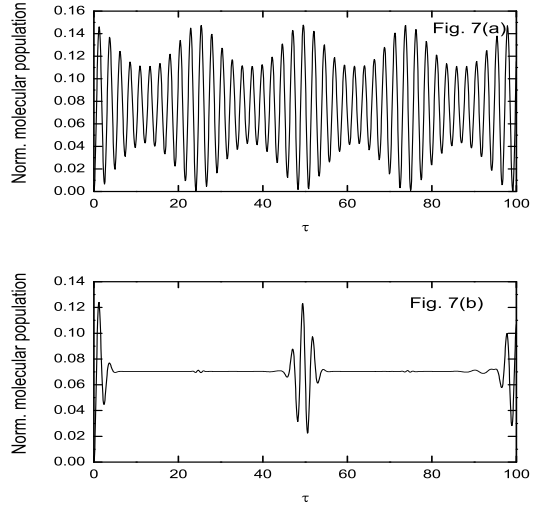


FIG. 7: Time evolution of the normalized molecular population for  $\chi/g = 0.1$  (a) Fock state with  $N = 20$  and  $d = 0$ . (b) Coherent state with  $\alpha = \beta = \sqrt{10}$ .

with mean particle number in both species of the atomic condensate 100. The solid line is the result from the mean-field theory, dashed line is the quantum solution with initially the Fock state and the dotted line symbolize the coherent state. One can see that the result from the Fock state and the coherent state display similar behavior, they deviate from the mean-field prediction with damping oscillation. The damping speed for the coherent state is faster than the Fock state and their phase coincide well. For numerical limitations we could not perform calculation with larger particle number. However as predicted in [18], for the zero-dimensional model, in their stochastic modeling with thousands of particle numbers, the result for coherent state and Fock state are almost indistinguishable. This means quantum statistical properties play less role as the particle number increases. The larger the particle number is, the system behaves more classically.

### III. QUANTUM CORRELATION AND STATISTICAL PROPERTIES

We are specifically interested in the case that initially the atomic condensate of different species are prepared in the  $SU(2)$  coherent state, which is a minimum uncertainty state with well-defined relative phase between the two species and can be experimentally created under suitable conditions [23]. The  $SU(2)$  coherent state can

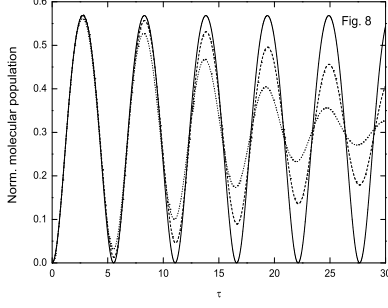


FIG. 8: Time evolution of the normalized molecular population for  $\chi/g = 0.01$  with mean-field prediction (solid line); Quantum solution with Fock state and  $N = 200$ ,  $d = 0$  (dashed line); Quantum solution with coherent state and  $\alpha = \beta = 10$  (dotted line).

be written in the Fock basis as

$$|\Psi\rangle_{SU(2)} = \sum_{n=0}^N \binom{N}{n}^{1/2} \left( \cos \frac{\theta}{2} \right)^n \left( \sin \frac{\theta}{2} \right)^{N-n} \times e^{i(N-n)\phi} |n\rangle_1 |N-n\rangle_2 \quad (25)$$

where the parameter  $\theta$  fixes the particle number in each species and  $\phi$  describes the relative phase between the two species. The mean population imbalance  $\langle D \rangle = N \cos \theta$  and we take  $\phi = 0$  in this paper for simplicity. In the case of  $\langle D \rangle = 0$  we studied the molecular dynamics with an initial  $SU(2)$  coherent state as well as the Fock state, which shows little difference. This means that the molecular dynamics mainly depends on the mean particle number of each atomic species. It will be interesting to investigate the joint quantum statistical properties of the atoms of different species for initially there exist anti-correlation between them as can be seen from Eq. (25). It can be estimated by the equal-time intensity correlation function

$$g_{12}^{(2)} = \frac{\langle N_1 N_2 \rangle}{\langle N_1 \rangle \langle N_2 \rangle} \quad (26)$$

when  $g_{12}^{(2)} = 1$ , the two species are uncorrelated;  $g_{12}^{(2)} > 1$  for correlation and  $g_{12}^{(2)} < 1$  for anti-correlation. In Fig. 9 we present the time evolution of  $g_{12}^{(2)}$  under different nonlinear interaction parameters, both for the Fock state and the  $SU(2)$  coherent state. From the figure one can see that correlation will always be developed between the two atomic species in the case of the Fock state. The correlation function for the  $SU(2)$  coherent state will be less than that for the Fock state during the time evolution. With increasing the nonlinear interaction parameters, the value of  $g_{12}^{(2)}$  will decrease. Especially in Fig. 9(c),  $g_{12}^{(2)}$  will always be less than 1 for the  $SU(2)$  coherent state during time development, which means the two atomic species are kept anti-correlated. It is convenient to study the quantum statistical properties of

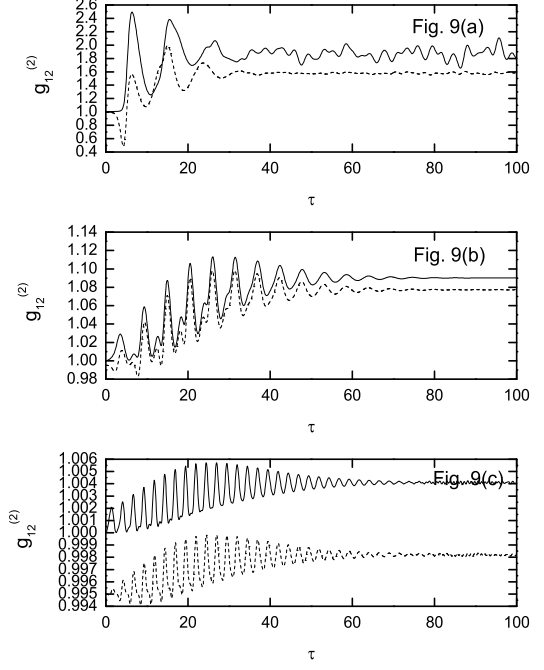


FIG. 9: Time evolution of the correlation function  $g_{12}^{(2)}$  for  $N = 200$ ,  $D = 0$  and (a)  $\chi/g = 0$ ; (b)  $\chi/g = 0.01$  and (b)  $\chi/g = 0.03$  for the Fock state (solid line) and the  $SU(2)$  coherent state (dashed line).

the matter wave field during dynamical evolution with the help of the phase-space quasiprobability distribution function [30, 31]. Here we introduce the  $Q$  function to describe the probability distribution of a quantum state of the matter wave field in phase space. The  $Q$  function of the particular mode is defined as

$$Q_i(\alpha) = \frac{1}{\pi} \langle \alpha | \rho_i | \alpha \rangle \quad (27)$$

where  $\rho_i$  is the reduced density operator of the  $i$  mode. We numerically simulate the  $Q$  function for the atomic mode and molecular mode with different initial states. The results are shown in Fig. 10 and Fig. 11. Fig. 10 gives the  $Q$  function for the atoms initially in the Fock state. For the Fock state does not have definite phase, one can see that the  $Q$  function always have the configuration of circular stripe, whose diameter changes with time development. Physically it corresponds to the exchange of particle numbers between the atomic and molecular mode. The case for the atoms initially in the coherent state is shown in Fig. 11. It is interesting to note that the shape of the contours are squeezed in some direction during time evolution. This means that the quantum fluctuations in the coherent matter wave field are redistributed in phase space due to the nonlinear interaction. The nonlinear terms in the Hamiltonian induce the self-phase and mutual-phase modulation of the

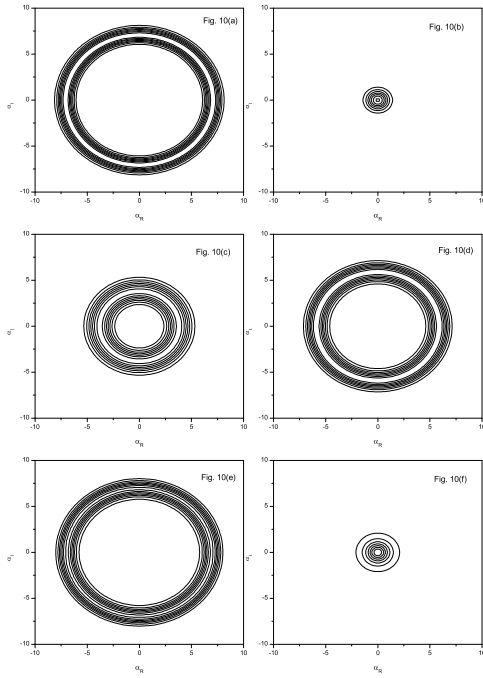


FIG. 10: Contours of the  $Q$  function of the atomic field (a)(c)(e) and molecular field (b)(d)(f) for the atoms are initially in the Fock state. The parameters are chosen as  $N = 100$ ,  $D = 0$ ,  $\chi/g = 0.01$  and for different time (a)(b)  $\tau = 0$ ; (c)(d)  $\tau = 3.2$  and (e)(f)  $\tau = 6.5$ .

matter wave field. The case for the  $SU(2)$  coherent state is very similar to that of the Fock state so we do not display it here.

#### IV. CONCLUSION

In conclusion, we have studied the dynamics of heteronuclear photoassociation of ultracold Bose atoms. Starting from the Hamiltonian (1), we derive the quantum Hamiltonian (7). We use the classical Hamiltonian (21) as an approximation to find the fixed points of the system and perform the stability analysis. It was found that population imbalance  $D$  between the two atomic species play an important role in the dynamics of the system. With larger  $D$ , the system would be more likely to be subject to modulational instability. The quantum Hamiltonian (7) is solved under the mean-field approximation in the limit of large particle numbers, the quantum solution is also presented. The difference between the two solutions are found and analyzed, we found

that the population imbalance  $D$  play similar role as the nonlinear parameter  $\Lambda$ . The effect of the quantum statistical properties of the initial atomic state is considered, it would affect the dynamics greatly with relatively small particle numbers. With the increasing of the parti-

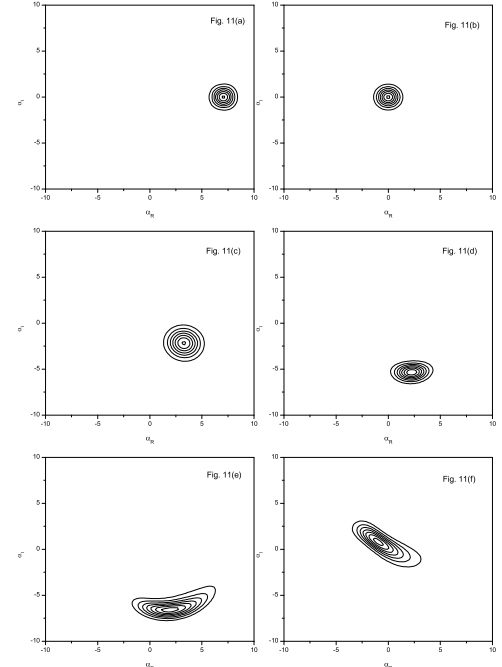


FIG. 11: Similar to Fig. 10 except that the atoms are initially in the coherent state with  $\alpha = \beta = 5\sqrt{2}$ .

cle number the system behaves more classically and the quantum statistical properties of the initial state play less important role. The intensity correlation function for the initial  $SU(2)$  coherent state are calculated, the two atomic species can be kept anti-correlated with appropriate parameters. We also numerically show that quantum statistical properties of the matter wave field changes due to the nonlinear interaction.

#### ACKNOWLEDGMENTS

This work is supported by the National Natural Science Foundation of China under Grant No. 10474055 and No. 10588402, by the Science and Technology Commission of Shanghai Municipality under Grant No. 04DZ14009 and No. 05PJ14038 (WZ), and by the US National Science Foundation (HP and HYL).

[1] C. A. Stan, M. W. Zwierlein, C. H. Schunck, S. M. F. Raupach and W. Ketterle, Phys. Rev. Lett. **93**, 143001

(2004).  
[2] S. Inouye, J. Goldwin, M. L. Olsen, C. Ticknor, J. L.

Bohn and D. S. Jin, Phys. Rev. Lett. **93**, 183201 (2004).

[3] C. Ospelkaus, S. Ospelkaus, L. Humbert, P. Ernst, K. Sengstock and K. Bongs, Phys. Rev. Lett. **97**, 120402 (2006).

[4] A. J. Kerman, J. M. Sage, S. Sainis, T. Bergeman and D. Demille, Phys. Rev. Lett. **92**, 153001 (2004).

[5] C. Haimberger, J. Kleinert, M. Bhattacharya and N. P. Bigelow, Phys. Rev. A **70**, 021402(R) (2004).

[6] D. Wang, J. Qi, M. F. Stone, O. Nikolayeva, H. Wang, B. Hattaway, S. D. Gensemer, P. L. Gould, E. E. Eyler, and W. C. Stwalley, Phys. Rev. Lett. **93**, 243005 (2004).

[7] H. Y. Ling, H. Pu and B. Seaman, Phys. Rev. Lett. **93**, 250403 (2004).

[8] S. J. J. M. F. Kokkelmans, H. M. J. Vissers and B. J. Verhaar, Phys. Rev. A **63**, 031601 (2001).

[9] M. Mackie, R. Kowalski and J. Javanainen, Phys. Rev. Lett. **84**, 3803 (2000).

[10] A. Nunnenkamp, D. Meiser and P. Meystre, New Journal of Physics **8**, 88 (2006).

[11] P. D. Drummond, K. V. Kheruntsyan and H. He, Phys. Rev. Lett. **81**, 3055 (1998).

[12] H. Uys, T. Miyakawa, D. Meiser and P. Meystre, Phys. Rev. A **72**, 053616 (2005).

[13] A. Ishkhanyan, G. P. Chernikov and H. Nakamura, Phys. Rev. A **70**, 053611 (2004).

[14] A. Vardi, V. A. Yurovsky and J. R. Anglin, Phys. Rev. A **64**, 063611 (2001).

[15] Y. Wu and R. Côté, Phys. Rev. A **65**, 053603 (2002).

[16] G.-R. Jin, C. K. Kim and K. Nahm, Phys. Rev. A **72**, 045602 (2005).

[17] G. Santos, A. Tonel, A. Foerster and J. Links, Phys. Rev. A **73**, 023609 (2006).

[18] M. K. Olsen, A. S. Bradley and S. B. Cavalcanti, Phys. Rev. A **70**, 033611 (2004).

[19] M. W. Jack and H. Pu, Phys. Rev. A **72**, 063625 (2005).

[20] Z.-D. Chen, J.-Q. Liang, S.-Q. Shen and W.-F. Xie, Phys. Rev. A **69**, 023611 (2004).

[21] L.-M. Kuang and Z.-W. Ouyang, Phys. Rev. A **61**, 023604 (2000).

[22] S. Choi and N. P. Bigelow, Phys. Rev. A **72**, 033612 (2005).

[23] D. Gordon and C. M. Savage, Phys. Rev. A **59**, 4623 (1999).

[24] H. Pu, W. Zhang, M. Wilkens and P. Meystre, Phys. Rev. Lett. **88**, 070408 (2002).

[25] G. Drobný, I. Jex and V. Bužek, Phys. Rev. A **48**, 569 (1993).

[26] K.-P. Marzlin and J. Audretsch, Phys. Rev. A **57**, 1333 (1998).

[27] G. J. Milburn, J. Corney, E. M. Wright and D. F. Walls, Phys. Rev. A **55**, 4318 (1997).

[28] Weiping Zhang and D. F. Walls, Phys. Rev. A **49**, 3799 (1994).

[29] C. K. Law, H. Pu and N. P. Bigelow, Phys. Rev. Lett. **81**, 5257 (1998).

[30] Weiping Zhang and D. F. Walls, Phys. Rev. A **52**, 4696 (1995).

[31] M. Greiner, O. Mandel, T. W. Hänsch and I. Bloch, Nature **419**, 51 (2002).